In Situ Magnetic Resonance Imaging of a Complete Supercapacitor Giving Additional Insight on the Role of Nanopores

Ghenima Oukali,[†,‡] Elodie Salager,[*,†,‡] Mohamed Ramzi Ammar,[‡] Charles-Emmanuel Dutoit,[†,‡] Vincent Sarou-Kanian,[†,‡] Patrice Simon,[†,∥] Encarnacion Raymundo-Piñero,[*,†,‡] and Michaël Deschamps[*,†,‡]

[†]Réseau sur le Stockage Électrochimique de l'Énergie (RS2E), CNRS FR3459, 33 rue Saint Leu, 80039 Amiens, France
[‡]CNRS, CEMHTI UPR3079, Orléans University, 1D avenue de la recherche scientifique, 45071 Orléans Cedex 2, France
[∥]Université Paul Sabatier, CIRIMAT UMR CNRS 5085, 118 route de Narbonne, 31062 Toulouse, France

ABSTRACT: **Nuclear magnetic resonance is one of the rare techniques able to probe selectively the ions inside the nanoporous network in supercapacitor devices. With a magnetic resonance imaging method able to detect all ions (adsorbed and nonadsorbed), we record one-dimensional concentration profiles of the active ions in supercapacitors with an electrode configuration close to that used in industry. Larger anionic concentration changes are probed upon charge and discharge in a carbide-derived carbon (CDC) with micropores smaller than 1 nm compared to a conventional nanoporous carbon (CC) with a larger distribution of pore sizes, up to 2 nm. They highlight the increased interaction of the anions with CDC and provide a better understanding of the enhanced capacitance in CDC-based supercapacitors.**

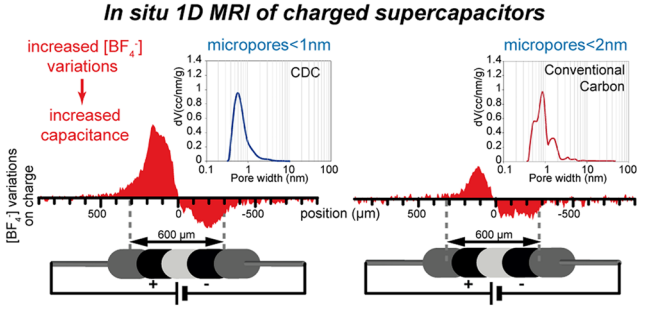

KEYWORDS: *supercapacitor, nanopore, carbon, nuclear magnetic resonance, magnetic resonance imaging*

The progression toward all-electric devices calls for ever-improving energy storage systems. Among them, carbon-based supercapacitors (electrochemical double layer capacitors) with organic electrolytes are emerging as powerful energy-saving devices with their extremely long cycle life and large specific powers.[1] The supercapacitor's energy storage mechanism relies on the electrostatic attraction between the electronic charges stored on a nanoporous material and the counterions of opposite charge in the electrolyte. The observation[2,3] of a large anomalous increase of the capacity for pore sizes smaller than 1 nm raised a lot of questions about the interactions between electronic charges, ions, and solvent molecules inside the nanoporous network but also about the influence of the active material structure in the adsorption and accommodation of ions and electronic charges. The full understanding of the electrolyte structure at the electrode/electrolyte interface is essential to achieve optimal performances.

Few experimental techniques are suitable for the characterization of a *full supercapacitor device*, such as those used on a commercial scale. Among them, electrochemical quartz crystal microbalance measurements provide *in situ* ionic fluxes and dynamics in electrodes under polarization.[4,5] Nuclear magnetic resonance (NMR) spectroscopy is one of the rare techniques capable of detecting selectively one species in the electrolyte to provide relative concentrations of adsorbed species, information on the local environment, or self-diffusion coefficients.[6−9]

RESULTS AND DISCUSSION

Ex situ solid-state NMR and exchange experiments[10] on nanoporous carbon electrodes charged in tetraethylammonium tetrafluoroborate in acetonitrile showed that the charging mechanism is based on ion exchanges at the positive and negative electrodes, where the counterion concentrations increase and the co-ions leave the carbon porous network. Nevertheless, the supercapacitor disassembly before each measurement leads to partial evaporation, which could distort the electrolyte structure. *In situ* experiments are needed to probe the functioning device, but the signal of the two

DOI: 10.1021/acsnano.9b04998

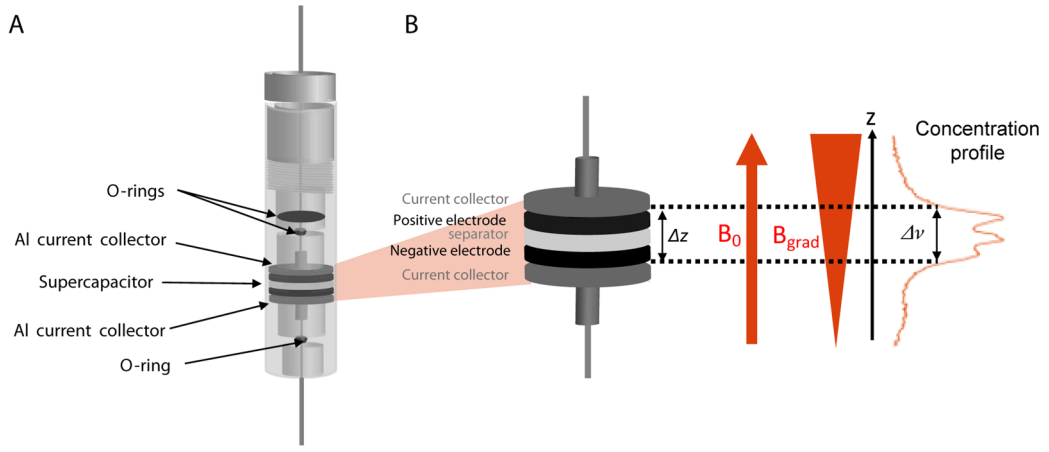

Figure 1. (A) *In situ* electrochemical cell containing the supercapacitor (5 mm diameter, 600 μm thickness once assembled). (B) Vertical ^{19}F spin density profile obtained from the ^{19}F NMR signal of the electrolyte.

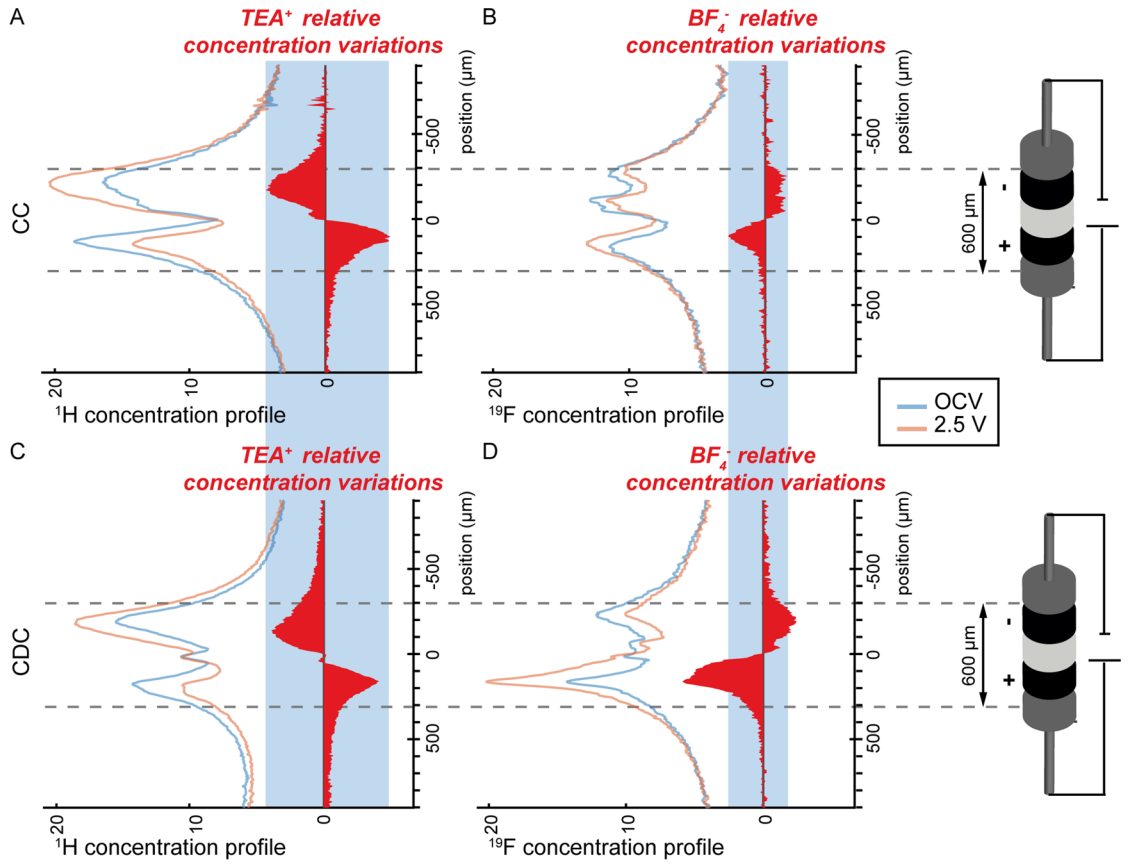

Figure 2. (A,C) ^{1}H and (B,D) ^{19}F 1D concentration profiles of a supercapacitor made of a CC (A,B) and CDC (C,D), during OCV before charging and at 2.5 V. The profiles of the concentration changes on charge (between 2.5 V and OCV) are displayed on the right of the profiles as filled red curves.

electrodes are overlapping in conventional NMR spectra. Spectra of individual electrodes can be recorded *in situ* using a shifted bagcell design with overlaid current collectors, so that a single electrode is inside the detection coil.[11,12] However, this design leads to degraded electrochemical performances mainly due to ohmic losses and transport issues (Figures S1 and S2).

The combination of NMR spectroscopy and magnetic resonance imaging (MRI) techniques with the classical chemical shift imaging (CSI) experiment appears as desirable to monitor changes *operando* in each electrode of a supercapacitor while maintaining good electrochemical performances.[13] The main issue with CSI experiments lies in the long echo time (>1 ms), which leads to signal loss from fast transverse relaxation. In this paper, we opt for an MRI method dedicated to ultrashort transverse relaxation times for the *in situ* study of a fully functioning supercapacitor, and we explore the effects of the carbon texture at the nanometer scale on the ion flux and charging mechanism by comparing a conventional nanoporous carbon (CC) and a carbide-derived carbon (CDC). The 1D concentration profiles along the vertical axis

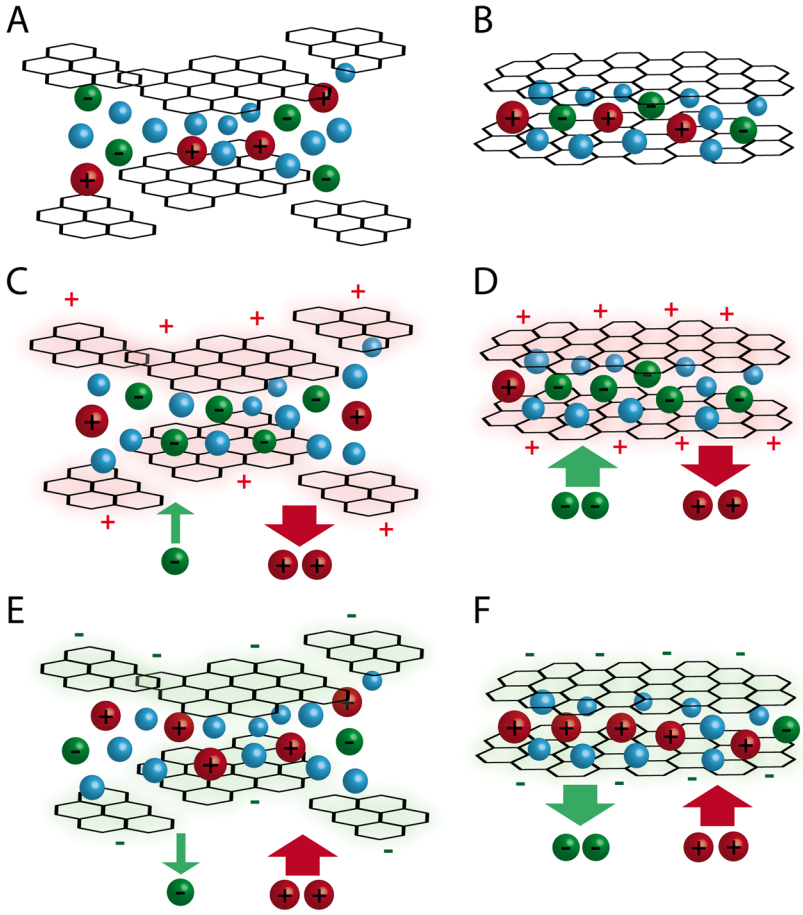

Figure 3. (A,B) Open-circuit contents of the pores for (left) CC and (right) CDC. The CC has both small and large nanopores, whereas the CDC has a majority of small nanopores, displayed here as slit-shaped spaces between carbon layers. Charge mechanism in (C,D) for the positive electrode and (E,F) for the green negative electrode, showing the observed anion and cation flux in the carbon electrode upon charging.

are recorded, and the relative variations in the concentration of the electrolyte ions can be compared, as the only experimental parameters that are changed are the carbon nature and the applied voltage (Figure 1).

It must be noted that quantitative measurements are difficult to achieve in NMR, as fast relaxation issues with paramagnetic centers, internal gradients, and changes in dielectric properties may lead to signal losses.

The better approach to overcome the signal loss due to short transverse relaxation (T_2 < 100s μs) consists of acquiring points in the *k*-space as soon as possible, that is, just after magnetization has been flipped in the transverse plane.[14−16] Experimentally, a short excitation pulse is applied with the gradient already switched on (Figure S5). The ^{1}H and ^{19}F NMR spectra spread over 5 kHz, so that strong magnetic pulsed field gradients are needed to achieve a relevant spatial resolution. The 1D concentration profile of the electrolyte in the supercapacitor is recorded with a spatial resolution of 70 μm using commercially available strong uniaxial pulsed magnetic field gradient systems (180 G/cm). However, the presence of the strong gradient does not allow us to distinguish adsorbed *versus* nonadsorbed species from the chemical shifts. We assume that far away from the electronic charges carried by the porous carbon, outside the porosity, the concentration should remain stable and homogeneous after a few minutes and over the duration of our experiments (*i.e.*, several hours) as electrolyte species diffuse rapidly. Therefore, the ion concentration changes we are observing result from the charge compensation phenomena inside the porosity, modifying the electrolyte structure at the nanometer scale.

Supercapacitors were tested with two carbons: the first, a conventional carbon (CC), is a commercially available nanoporous carbon, and the second one, CDC, is a carbon derived from titanium carbide.[2] The structural organization of the CC is slightly higher than that of the CDC from Raman spectroscopy (Figure S3). Importantly, the micropore size distribution reaches 2 nm for CC, whereas CDC features mainly micropores smaller than 1 nm (Figure S4 and Table S1). As expected, the supercapacitor made with CDC displays a capacitance of about 125 F/g (25% increase from CC).

All electrodes are prepared by spreading a paste of nanoporous carbon powder (85 w%), polytetrafluoroethylene (PTFE) binder (10 w%), and carbon black (5 w%). The 5 mm diameter, 170 μm thick electrodes are punched out and assembled with two 200 μm thick glass fiber separators in an electrochemical cell suitable for NMR measurements[17] and soaked with organic electrolyte: a 1 mol·L^{-1} solution of tetraethylammonium tetrafluoroborate (TEA^+/BF_4^-) in deuterated acetonitrile. We followed the modifications of the cationic (^{1}H) and anionic (^{19}F) concentration profiles during charge and discharge. In both cases, a concentration profile was recorded with no applied voltage (open-circuit voltage, OCV,

conditions) for an overview of the initial distribution of ions. Then, the supercapacitor was charged to 2.5 V and maintained at that voltage for the duration of a second measurement of the concentration profile (2−3 h). The supercapacitor was then discharged and maintained at 0 V for the third profile.

The concentration profiles for OCV and 2.5 V (Figure 2) contain contributions from the electrolyte species (TEA^+ or BF_4^-) inside the electrodes and the separator and from residues on the cell walls and the current collectors. There is also a small broad signal from the PTFE binder and the Kel-F polymer (PCTFE or polychlorotrifluoroethylene) of the cell in ^{19}F profiles or from residual protons in the carbons for ^1H profiles. Deuterated acetonitrile was used, and therefore, the solvent was never detected in these ^1H profiles. The variations in TEA^+ and BF_4^- concentrations are visualized by subtracting the profiles and are displayed as filled red curves on the right of each profile in Figure 2, using the same scale (see the Supporting Information for the definition of the scale). This procedure also removes the undesired contributions, which are expected to remain unchanged during the experiments. Note that the increase in the shift of the adsorbed species observed upon charging and alignment issues between the supercapacitor axis and the *z*-pulsed field gradient may result in partial overlap of the contributions of the spins inside the electrodes and the separator.

We detected a reproducible and reversible increase in the total signal area at 2.5 V of about 6 and 3% in the case of ^1H and ^{19}F, respectively. We could not assign them to changes in transverse or longitudinal relaxation times; they are probably due to a conductivity decrease upon charging, which results in an improvement of the probe quality factor and an increase of the overall signal.[18] To account for this small effect, we adjusted the intensity of the whole profile to keep the total signal identical for the three states of charge (Figure S6).

In CC (Figure 2A,B), the ^1H and ^{19}F relative concentration changes show ion exchange during charging: upon charging, TEA^+ migrate toward the negative electrode and are ejected from the positive electrode. At the same time, the BF_4^- population at the negative electrode decreases slightly, whereas it increases in similar proportions into the positive electrode.

Those experiments evidence some ion exchange at both electrodes (counterions, co-ions out), in agreement with previous reports.[10,19] However, compared to the flow of cations, the flux of anions is reduced. The mechanism at the negative electrode is therefore counterion adsorption with a small contribution from anion desorption (*i.e.*, from ion exchange), which also confirms previous results.[19] At the positive electrode, there is co-ion desorption (TEA^+) and a small influx of counterions (BF_4^-).

On discharge, the relative concentration changes (filled orange in Figure S7) display the reverse behavior. In addition, the similar concentration profiles (at 0 V and OCV) indicate a good reversibility of the charge of the supercapacitor. This is in agreement with the previous observations by *ex situ* NMR experiments.[10]

The carbide-derived carbon was then studied with *in situ* ^1H and ^{19}F 1D MRI. The relative ionic concentration profiles, normalized to the same area, are reported in Figure 2C,D. Interestingly, the relative concentration changes in TEA^+ and BF_4^- are of similar shape in both carbons, but we detect an increased interaction with the anions in CDC (Figure 2D) compared to that in CC. The charge−discharge mechanism is therefore more tilted toward ion exchange with now an increase flux of anions, out of the negative electrode and into the positive one (Figure 3).

These differences can be rationalized with the carbon texture. The ions located in the small or sub-nanometer micropores are considered as the key players for the anomalous increase of capacitance in nanoporous carbon electrodes,[2,3] and we provide here an experimental probe for this behavior.

In conventional activated carbons (like CC), before any charge, the TEA^+ are spontaneously in excess inside the small micropores, whereas the anions are rather located nearby, in the connected larger micropores, that is, 1−2 nm (Figure 3A). This is clearly seen from previously published ^{13}C and ^{11}B NMR spectra of the same carbon soaked with a similar electrolyte solution: there are 3 times more TEA^+ than BF_4^- adsorbed in the micropores (without any voltage being applied), which are both identified from their signals shifted by −6 to −8 ppm in the NMR spectrum.[10] This preferential adsorption of TEA^+ may result from their hydrophobic ethyl groups and explain the dissymmetric behavior of these electrodes. This localized violation of electroneutrality has also been observed by NMR in aqueous electrolytes.[20] As there is less BF_4^- adsorbed in the smallest micropores, these anions are less likely to be repelled by electronic negative charges (Figure 3E), and the anion flux is therefore limited (Figure 3C). This is possible because the BF_4^- anions can reside in the large micropores close the small ones to maintain electroneutrality at the nanometer scale, while staying slightly away from the carbon surface, as seen from their larger unshifted NMR signal in soaked electrodes. This may be also linked to a stronger affinity for the acetonitrile molecules, which may prevent them from entering the smallest micropores. All in all, the longer distance to the carbon surface is likely to result in lesser electrostatic interactions with anions upon charging. However, we cannot exclude a reorganization of the anions inside the positive electrode, where previously free anions can then enter the smaller pores, replacing the exiting cations. However, we expect the quantity of incoming anions to be limited to what is available in nearby large nanopores and what is expelled from the negative electrode.

In CDC, the large proportion of small micropores is considered as the driving force behind increased capacitance.[21,22] It favors the joint adsorption of cations and anions, and we infer this from the similar ^{19}F and ^1H *ex situ* NMR spectra of a very similar CDC carbon soaked with $TEABF_4$ in deuterated acetonitrile in ref 23 (Figure 3B). These previously published NMR spectra clearly show a very close proportion of adsorbed species for cations and anions, which hints toward a symmetric behavior for anions and cations upon charging/discharging this CDC-based supercapacitor. This might be expected in CDC, as the narrower pore size distribution will force anions to also come close to the carbon surface, as larger micropores are not available. Therefore, BF_4^- anions are now attracted/repelled by the electronic charge in the same proportions as TEA^+ cations (Figure 3B,D). Therefore, in both electrodes, the ion exchange mechanism dominates with similar contributions from the cations and anions.

We also recorded the ^1H profile for a supercapacitor made with CC and a 1 $mol{\cdot}L^{-1}$ solution of $TEABF_4$ in non-deuterated acetonitrile to probe the solvent's part in the process (Figure 4A). As expected, the ^1H concentration profile contains a contribution from the solvent. The ^1H concentration changes are, however, of the same order of magnitude as those observed for TEA^+ alone (Figure 4B). Although we

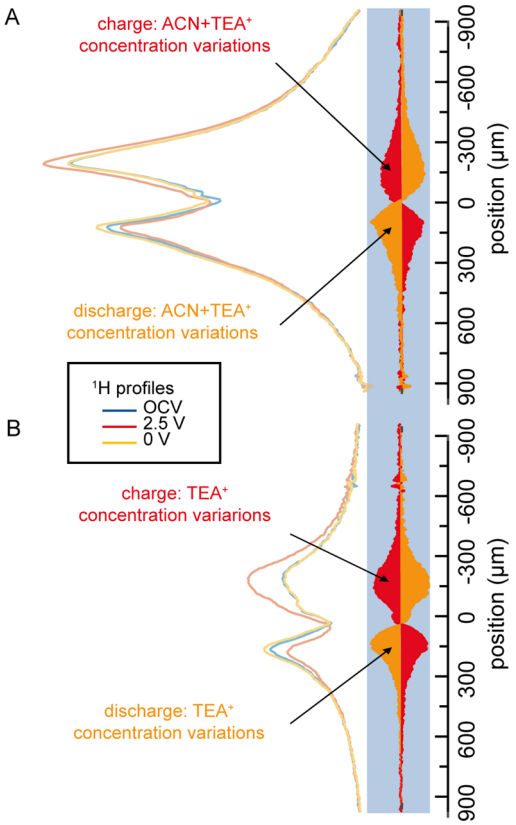

Figure 4. Charge/discharge 1D TEA^+ concentration profiles (left) during OCV, at 2.5 and 0 V, and the corresponding changes on the same scale (right: red for charge and orange for discharge) observed for a supercapacitor made with CC with (A) non-deuterated and (B) deuterated acetonitrile.

cannot rule out a rearrangement of the solvent at the nanometer scale, nor that small changes in solvent concentrations are harder to detect, we can safely assume that no significant macroscopic change in the solvent concentration occurs in the electrodes, which agrees well with previous results from electrochemical quartz crystal microbalance measurements.[5] This also implies that we do not see a flux of solvents molecules resulting from desolvation. Although desolvation was inferred from the relative size of pores and solvated/desolvated ions[2] and confirmed with the decrease of the adsorbed NMR solvent signal at the negative electrode in previous experiments,[10] our results indicate that the solvent molecules stay in the vicinity of adsorbed ions.

CONCLUSIONS

As a conclusion, we managed with a 1D MRI analysis to follow the ionic concentration changes in supercapacitors with an electrode configuration close to that used in industry and with good electrochemical performances. The strong magnetic field gradient (180 G/cm) allows for the monitoring of the flux of ions in and out of each electrode. In a microporous carbon with a large pore size distribution from 0.5 to 2.0 nm as in a conventional carbon, our MRI measurements indicate TEA^+ adsorption at the negative electrode and desorption at the positive electrode, whereas the BF_4^- opposite flux is observed in lesser proportions. In a microporous carbon with a narrow pore size distribution around 0.7 nm (CDC), we see an increased interaction with the anions, which tilts the charge mechanism, in both electrodes, toward ion exchange, with counterions entering and co-ions leaving each electrode.

We explain this phenomenon by the porous texture of CDC: cations and anions are now in equal concentration in the small micropores because of the absence of large micropores, which leads to a more symmetrical behavior of the ions during charge and discharge and an increased capacitance.

The present method is applicable to the *operando* studies of various devices (batteries, fuel cells, electrochemical cells, *etc.*) by magnetic resonance imaging.

METHODS

Electrode Preparation. The electrodes are prepared by spreading the paste of nanoporous carbon powder (85 w%) mixed with a PTFE binder (10 w%, Aldrich) and carbon black (5 w%, Pure Black, Superior Graphite Co., USA). The 5 mm diameter, 170 μm thick electrodes are punched out and assembled with two 200 μm thick glass fiber separators (Whatman) in an electrochemical cell suitable for NMR measurements[17] and soaked with an organic electrolyte: a 1 $mol{\cdot}L^{-1}$ solution of tetraethylammonium (TEA^+)−tetrafluoroborate (BF_4^-) in deuterated acetonitrile—all purchased from Sigma-Aldrich and used without further purification.

Electrochemical Cycling. The supercapacitors are preconditioned before the NMR experiments: the cells are cycled five times at a rate of 2 $mV{\cdot}s^{-1}$ between 0.9 and 1.1 V then five times between 0.9 and 1.3 V and so on until reaching 2.5 V. The first NMR profile measurement is carried out in open-circuit voltage conditions for an overview of the species distribution (cations or anions) before charging. The supercapacitor is then charged with a rate of 2 $mV{\cdot}s^{-1}$ to 2.5 V and held floating at this voltage to perform the second NMR profile measurement (supercapacitor in charge) for approximately 3 h. The supercapacitor is then discharged at the same rate (2 $mV{\cdot}s^{-1}$) and held floating at 0 V for approximately 3 h during the third NMR profile measurement corresponding to the discharged state.

To that end, we set up a potentiostat and NMR spectrometer synchronization. A cable connects the potentiostat with the NMR spectrometer (IPSO card). The potentiostat sends a TTL pulse once the desired voltage is reached. The NMR pulse sequence is modified to include a waiting time for this TTL pulse before the measurement starts.

1D Concentration Profile Recording. Experimentally, a short excitation pulse is applied with the gradient already switched on (see Figure S5). This MRI experiment is identical to that originally proposed by Lauterbur,[14] later renamed BLAST[15] or ZTE.[16] The name only differs because of the data processing (2D or 3D image reconstruction). We record the 1D concentration profile along the vertical axis, which is obtained from a simple Fourier transform of the data. The missing points (=2) in the center of the *k*-space due to the dead time of the probe are not numerically calculated. The pulse sequence allows for a significant reduction of the delay between excitation and acquisition. Yet the short dead time (TE) still creates a first-order phase shift and has a significant effect on the concentration profiles and their differences. The concentration profiles were therefore processed in magnitude mode. The 1D concentration profiles were measured with the pulse sequence shown in Figure S5 on a Bruker 200 MHz wide bore Avance III spectrometer equipped with a Bruker Diff30 probe (^1H and ^{19}F 10 mm inner diameter saddle coils) and a GREAT60 (60 $G{\cdot}A^{-1}{\cdot}cm^{-1}$) gradient amplifier. The strength of the pulsed magnetic field gradient was ramped up to 180 $G{\cdot}cm^{-1}$ in 500 μs and stabilized for 1 ms before a 30° hard pulse excitation with a duration of 3.5 μs (25 W). The probe dead time (TE) is set to 6.5 μs, and the signal is recorded for 2 ms. For the ^1H concentration profiles, a recovery delay of 5 s was sufficient to ensure the complete relaxation of the spin system, and 2048 scans were used for each concentration profile. For the ^{19}F concentration profiles, a recovery delay of 10 s was necessary and 1024 scans per concentration profile were recorded. The spin density profiles for ^1H and ^{19}F spread over a frequency of around 46 kHz. The resolution is limited by the

width of the spectrum under no gradient (5 kHz), corresponding to around 70 μm in ^{1}H and ^{19}F.

ASSOCIATED CONTENT

Supporting Information

The Supporting Information is available free of charge on the ACS Publications website at DOI: 10.1021/acsnano.9b04998.

Electrochemical and *ex situ* NMR characterization of the supercapacitor designs, structural characterization of the carbons, details on experimental and processing procedures, concentration profiles and changes on discharge (PDF)

AUTHOR INFORMATION

Corresponding Authors

*E-mail: elodie.salager@cnrs-orleans.fr.
*E-mail: raymundo@cnrs-orleans.fr.
*E-mail: michael.deschamps@univ-orleans.fr.

ORCID

Elodie Salager: 0000-0002-5443-9698
Patrice Simon: 0000-0002-0461-8268
Encarnacion Raymundo-Piñero: 0000-0001-9712-3987
Michaël Deschamps: 0000-0001-8309-3932

Notes

The authors declare no competing financial interest.

ACKNOWLEDGMENTS

The authors acknowledge financial support from the French national network "Réseau sur le Stockage Electrochimique de l'Energie" (RS2E) FR CNRS 3459, and from Laboratory of Excellence program STORE-EX (ANR 10-LABX-0076). G.O. thanks the Agence Nationale de la Recherche (ANR) with the LABEX STORE-EX (ANR-10-LABX-76) for Ph.D. funding.

REFERENCES

(1) Miller, J. R.; Burke, A. F. Electrochemical Capacitors: Challenges and Opportunities for Real-World Applications. *Electrochem. Soc. Interface* **2008**, *17*, 53−57.
(2) Chmiola, J.; Yushin, G.; Gogotsi, Y.; Portet, C.; Simon, P.; Taberna, P. L. Anomalous Increase in Carbon Capacitance at Pore Sizes Less Than 1 Nanometer. *Science* **2006**, *313*, 1760−1763.
(3) Raymundo-Piñero, E.; Kierzek, K.; Machnikowski, J.; Béguin, F. Relationship between the Nanoporous Texture of Activated Carbons and Their Capacitance Properties in Different Electrolytes. *Carbon* **2006**, *44*, 2498−2507.
(4) Levi, M. D.; Levy, N.; Sigalov, S.; Salitra, G.; Aurbach, D.; Maier, J. Electrochemical Quartz Crystal Microbalance (EQCM) Studies of Ions and Solvents Insertion into Highly Porous Activated Carbons. *J. Am. Chem. Soc.* **2010**, *132*, 13220−13222.
(5) Tsai, W.-Y.; Taberna, P.-L.; Simon, P. Electrochemical Quartz Crystal Microbalance (EQCM) Study of Ion Dynamics in Nanoporous Carbons. *J. Am. Chem. Soc.* **2014**, *136*, 8722−8728.
(6) Lee, S.-I.; Saito, K.; Kanehashi, K.; Hatakeyama, M.; Mitani, S.; Yoon, S.-H.; Korai, Y.; Mochida, I. ^{11}B NMR Study of the BF_4^- Anion in Activated Carbons at Various Stages of Charge of EDLCs in Organic Electrolyte. *Carbon* **2006**, *44*, 2578−2586.
(7) Borchardt, L.; Oschatz, M.; Paasch, S.; Kaskel, S.; Brunner, E. Interaction of Electrolyte Molecules with Carbon Materials of Well-Defined Porosity: Characterization by Solid-State NMR Spectroscopy. *Phys. Chem. Chem. Phys.* **2013**, *15*, 15177−15184.
(8) Forse, A. C.; Griffin, J. M.; Presser, V.; Gogotsi, Y.; Grey, C. P. Ring Current Effects: Factors Affecting the NMR Chemical Shift of Molecules Adsorbed on Porous Carbons. *J. Phys. Chem. C* **2014**, *118*, 7508−7514.
(9) Forse, A. C.; Griffin, J. M.; Merlet, C.; Carretero-Gonzalez, J.; Raji, A.-R. O.; Trease, N. M.; Grey, C. P. Direct Observation of Ion Dynamics in Supercapacitor Electrodes Using *In Situ* Diffusion NMR Spectroscopy. *Nat. Energy* **2017**, *2*, 16216.
(10) Deschamps, M.; Gilbert, E.; Azais, P.; Raymundo-Piñero, E.; Ammar, M. R.; Simon, P.; Massiot, D.; Béguin, F. Exploring Electrolyte Organization in Supercapacitor Electrodes with Solid-State NMR. *Nat. Mater.* **2013**, *12*, 351−358.
(11) Wang, H.; Köster, T. K.-J.; Trease, N. M.; Ségalini, J.; Taberna, P.-L.; Simon, P.; Gogotsi, Y.; Grey, C. P. Real-Time NMR Studies of Electrochemical Double-Layer Capacitors. *J. Am. Chem. Soc.* **2011**, *133*, 19270−19273.
(12) Wang, H.; Forse, A. C.; Griffin, J. M.; Trease, N. M.; Trognko, L.; Taberna, P.-L.; Simon, P.; Grey, C. P. *In Situ* NMR Spectroscopy of Supercapacitors: Insight into the Charge Storage Mechanism. *J. Am. Chem. Soc.* **2013**, *135*, 18968−18980.
(13) Ilott, A. J.; Trease, N. M.; Grey, C. P.; Jerschow, A. Multinuclear *In Situ* Magnetic Resonance Imaging of Electrochemical Double-Layer Capacitors. *Nat. Commun.* **2014**, *5*, 4536.
(14) Lauterbur, P. C. Image Formation by Induced Local Interactions: Examples Employing Nuclear Magnetic Resonance. *Nature* **1973**, *242*, 190−191.
(15) Hafner, S. Fast Imaging in Liquids and Solids with the Back-Projection Low Angle ShoT (BLAST) Technique. *Magn. Reson. Imaging* **1994**, *12*, 1047−1051.
(16) Weiger, M.; Pruessmann, K. P.; Hennel, F. MRI with Zero Echo Time: Hard *versus* Sweep Pulse Excitation. *Magn. Reson. Med.* **2011**, *66*, 379−389.
(17) Salager, E.; Sarou-Kanian, V.; Sathiya, M.; Tang, M.; Leriche, J.-B.; Melin, P.; Wang, Z.; Vezin, H.; Bessada, C.; Deschamps, M.; Tarascon, J.-M. Solid-State NMR of the Family of Positive Electrode Materials $Li_2Ru_{1-Y}Sn_YO_3$ for Lithium-Ion Batteries. *Chem. Mater.* **2014**, *26*, 7009−7019.
(18) Houlleberghs, M.; Hoffmann, A.; Dom, D.; Kirschhock, C. E. A.; Taulelle, F.; Martens, J. A.; Breynaert, E. Absolute Quantification of Water in Microporous Solids with ^{1}H Magic Angle Spinning NMR and Standard Addition. *Anal. Chem.* **2017**, *89*, 6940−6943.
(19) Griffin, J. M.; Forse, A. C.; Tsai, W.-Y.; Taberna, P.-L.; Simon, P.; Grey, C. P. *In Situ* NMR and Electrochemical Quartz Crystal Microbalance Techniques Reveal the Structure of the Electrical Double Layer in Supercapacitors. *Nat. Mater.* **2015**, *14*, 812−819.
(20) Luo, Z.-X.; Xing, Y.-Z.; Ling, Y.-C.; Kleinhammes, A.; Wu, Y. Electroneutrality Breakdown and Specific Ion Effects in Nanoconfined Aqueous Electrolytes Observed by NMR. *Nat. Commun.* **2015**, *6*, 6358.
(21) Futamura, R.; Iiyama, T.; Takasaki, Y.; Gogotsi, Y.; Biggs, M. J.; Salanne, M.; Ségalini, J.; Simon, P.; Kaneko, K. Partial Breaking of the Coulombic Ordering of Ionic Liquids Confined in Carbon Nanopores. *Nat. Mater.* **2017**, *16*, 1225−1232.
(22) Salanne, M.; Rotenberg, B.; Naoi, K.; Kaneko, K.; Taberna, P.-L.; Grey, C. P.; Dunn, B.; Simon, P. Efficient Storage Mechanisms for Building Better Supercapacitors. *Nat. Energy* **2016**, *1*, 16070.
(23) Forse, A. C.; Griffin, J. M.; Wang, H.; Trease, N. M.; Presser, V.; Gogotsi, Y.; Simon, P.; Grey, C. P. Nuclear Magnetic Resonance Study of Ion Adsorption on Microporous Carbide-Derived Carbon. *Phys. Chem. Chem. Phys.* **2013**, *15*, 7722.

Supplementary Information

In Situ Magnetic Resonance Imaging of a Complete Supercapacitor Giving Additional Insight on the Role of Nanopores

Ghenima Oukali,[†,‡] Elodie Salager,[†,‡,*] Mohamed Ramzi Ammar,[‡] Charles-Emmanuel Dutoit,[†,‡] Vincent Sarou-Kanian,[†,‡] Patrice Simon,[†,||] Encarnacion Raymundo-Piñero,[†,‡,*] Michaël Deschamps[†,‡,*]

[†] Réseau sur le Stockage Electrochimique de l'Energie (RS2E), CNRS FR3459, 33 rue Saint Leu, 80039 Amiens, France

[‡] CNRS, CEMHTI UPR3079, Université d'Orléans, 1D avenue de la recherche scientifique, 45071 Orléans Cedex 2, France

[||] Université Paul Sabatier, CIRIMAT UMR CNRS 5085, 118 route de Narbonne, 31062 Toulouse, France

Electrodes configuration effect

Electrochemical study

We performed cyclic voltammetry experiments on several supercapacitor configurations (figure S1) to compare their performances. We observed that the conventional parallel configuration provides the greatest capacity with a nearly rectangular voltammogram while shifted electrodes display degraded performances. The charge stored on the electrode surface is reduced as the electrode contact surface decreases. This implies that for a given applied voltage, we expect that the amount of immobilized counter-ions and the electric potential will vary inside the electrodes and that their charged state may lead to inhomogeneous ion concentrations.

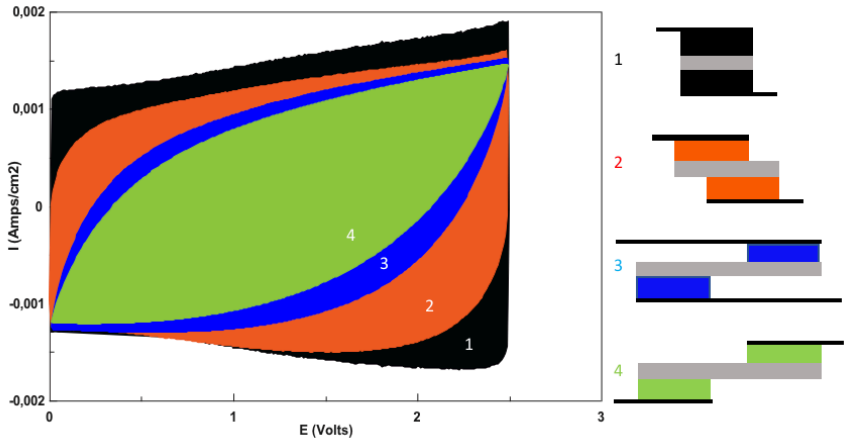

Figure S1. Cyclic voltammetry of different supercapacitors, with (1) conventional parallel configuration (black), (2) with slightly shifted electrodes (orange), (3) with shifted electrodes and overlapping current collectors (blue) and (4) shifted electrodes and no overlapping current collectors.

Ex situ Nuclear Magnetic Resonance (NMR) study

^{11}B *ex situ* Magic Angle Spinning (MAS)-NMR spectra were recorded in order to characterize the effect of the supercapacitor cell configuration on the proportion of ions stored inside the electrodes. The electronic density on the carbon was shown to affect the resonance frequency of adsorbed species.[1] DFT calculations showed that the addition or removal of electrons to a delocalized system induces considerable changes in the NMR shift of nearby spins.[2]

Figure S2 shows the *ex situ* ^{11}B MAS-NMR spectra of positive and negative electrodes for three supercapacitor cell designs, after each were charged at 2.5 V (at a rate of 2 mV/s) and disassembled straight after the charge. The electrode material was detached from the current collectors and placed inside a 4 mm rotor. The sample spinning rate was set to 5 kHz and 1D spectra were recorded in a Bruker 200 MHz Avance HD spectrometer equipped with a 4 mm WVT ^{1}H-^{19}F/X double resonance probe, using a long recovery delay of 20 s to ensure full relaxation of the spin system.

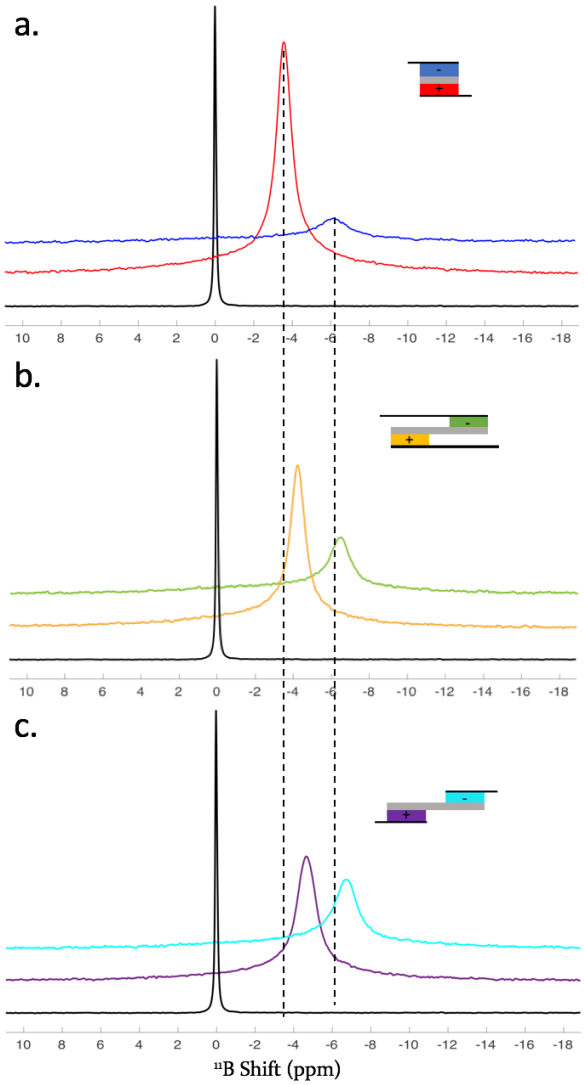

Figure S2. *Ex situ* ^{11}B MAS-NMR spectra of the positive and negative electrodes of different supercapacitor cell designs charged at 2.5 V (schemes displayed on the right-hand side of each spectrum). (a) conventional parallel configuration, (b) design with shifted electrodes and overlapping current collectors and (c) design featuring shifted electrodes and no overlap of the current collectors. The spectrum obtained for the free electrolyte is shown in black for reference. The dashed lines are guides for the eye.

The conventional design, the "long cell design" and the overlaid cell design introduced by Wang et al.[3] for easier *in situ* NMR experiment were tested. All the NMR spectra display a peak corresponding to BF_4^- anions in the electrode porosity after charging. The first observation concerns the differences in peak intensities between the positive electrode (larger peak) and the negative electrode (smaller peak): as expected, the positive electrode contains more anions. The more resistive designs display a lesser difference in intensities, which reflect their lower electronic charges in agreement with the voltammograms. This is

confirmed by the peak positions. Inside the porosity, the chemical shift is modified by -6 ppm/-8 ppm. This effect is reduced upon charging.[2] The peak for the anions in the parallel design is closer to the electrolyte peak compared to the other designs and confirms the larger electronic density reached in the electrodes of the conventional design.

CC and CDC structural characterisation

Two types of carbons were used: the first, (CC), is a commercially available nanoporous carbon (Norit (Cabot) DLC Super 50) and the second one (CDC) is a carbon derived from titanium carbide, chlorinated at 900°C.[4]

Structural study by Raman scattering

Vibrational Raman studies were performed in ambient conditions using a Renishaw Invia Reflex spectrometer equipped with an Ar^+ laser source (2.41eV/514.5nm). The spectra were collected under a Leica DM2500 optical microscope (×50 objectives/N.A.= 0.75). Very low incident power (~1mW) was used to avoid heating effects or a possible modification of the local structural organization.

The Raman spectrum of Highly Oriented Pyrolytic Graphite is used here as a reference and it is characterized by symmetry-allowed modes. The band located at 1581cm^{-1} (the G band) corresponds to one-phonon Raman scattering process at the 1st Brillouin zone center Γ (q~0, q stands for the phonon wavevector) and consists of the collective in-plane bond stretching of the polyaromatic carbon atoms (E_{2g} symmetry). The band located at around 2700 cm^{-1} (The so-called G' or 2D band), appearing as a doublet, corresponds to the totally symmetric transversal phonon A'_1 located in the vicinity of the high symmetry phonon points (K or K'). The activation of this mode is satisfied by the scattering by two phonons with opposite wavevector (q≠0). The doublet is generally the signature of tri-periodic structure of graphene layers.

Disordered sp^2 carbons are characterized by the appearance the so-called D band, in the first-order Raman spectrum, located at around 1350 cm^{-1}. It is the first order of the G' or 2D band requiring defects to be activated. At relatively low defect density, the D band intensity increases with increasing disorder. This is accompanied by the increase of the width of the Raman bands as well as the weakening of the second order bands.

The analysis of the Raman spectra (Figure S3) indicates, based on those parameters, that the structural organization of C is slightly higher than the CDC.

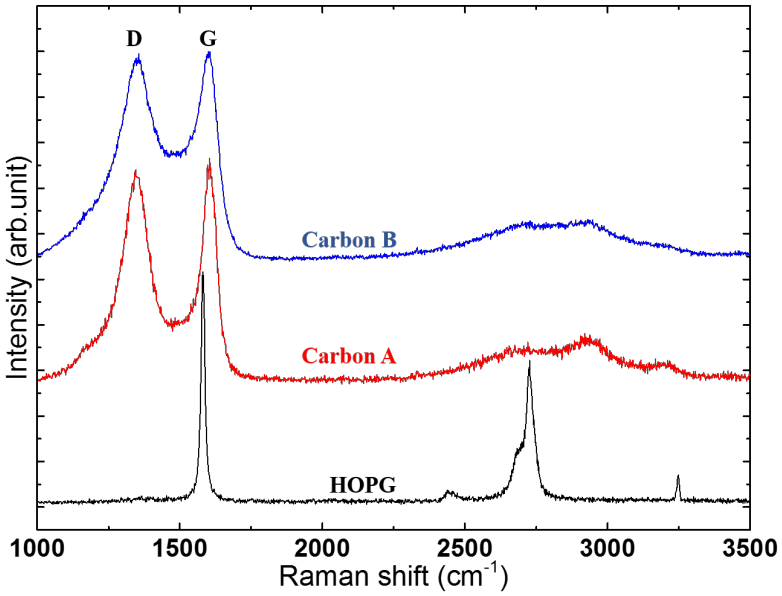

Figure S3. Raman spectra obtained for CC (carbon A - red) and CDC (carbon B - blue), using a laser energy of 2.41 eV (514.5 nm). The spectrum of HOPG (Highly oriented pyrolytic graphite) is displayed as a reference in black.

Pore size distribution

The specific surfaces area and pore size distributions for the two carbone were obtained from the N_2 and CO_2 adsorption isotherms at 77 K and 273 K, respectively. The total surface area (S_{BET}) was obtained from the N_2 isotherm with the BET equation, the specific microporous surface (S_{DR}) and ultramicropore volume ($V_{ultramicro}$) were obtained by applying the Dubinin-Raduskevich equation to the CO_2 isotherm. The micropore (V_{micro}) and mesopore (V_{meso}) volumes were determined from the N_2 isotherm using the Nonlinear Differential Functional Theory pore size distribution (2D-NLDFT) assuming an energetic heterogeneity of carbon pores.[5]

The pore size distribution is ranging from micro- to meso-pores for CC(carbon A – red), whereas CDC (carbon B - blue) features mainly micropores under 1 nm and a very little amount of large micropores and mesopores (Figure S4 and Table S1).

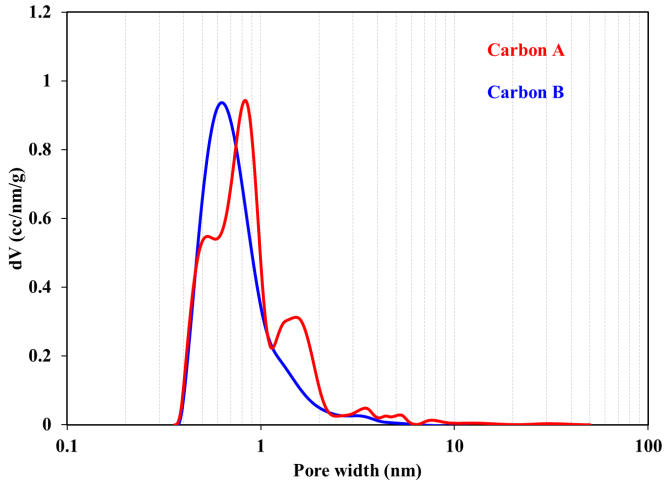

Figure S4. 2D-NLDFT Pore size distribution of a conventional carbon (CC : carbon A, in red) and a carbide derived carbon (CDC: carbon B in blue).

Table S1. Structural properties of conventional carbon (CC) and CDC

	Origin	$S_{BET}(N_2)$ m^2/g	$S_{DR}(CO_2)$ m^2/g	$V_{ultramicro}$ [a] (d<0.7nm) cm^3/g	V_{micro} [b] (d<1nm) cm^3/g	V_{micro} [b] (1<d<2nm) cm^3/g	V_{meso} [b] (2<d<50nm) cm^3/g
CC	From coconut fiber, carbonized and activated with H_2O	1560	1519	0.58	0.36	0.30	0.22
CDC	Derived from titanium carbide generated by chlorination : $TiC + 2Cl_2 \rightarrow TiCl_4 + C$	1489	1602	0.61	0.51	0.10	0.09

a: obtained after applying Dubinin-Radushkevich equation to the CO_2 adsorption data
b: obtained after applying the 2D-NLDFT method to the N_2 adsorption data

1D concentration profile recording

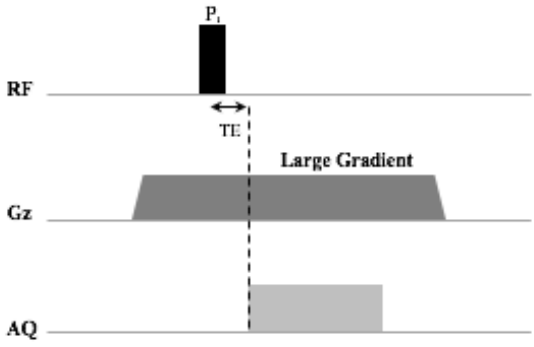

Figure S5. Pulse sequence used for the measurement of the 1D concentration profiles.

Calculation of the profiles of concentration change

The concentration spatial variations were calculated by difference of the concentration profiles in magnitude mode. The concentration profiles display an overall increased area upon charging, seemingly due to a small decrease in the overall conductivity and an improved probe quality factor. We scaled down the overall area of the concentration profiles at 2.5 V and 0 V to compensate for these variations, as shown in Figure S6 below.

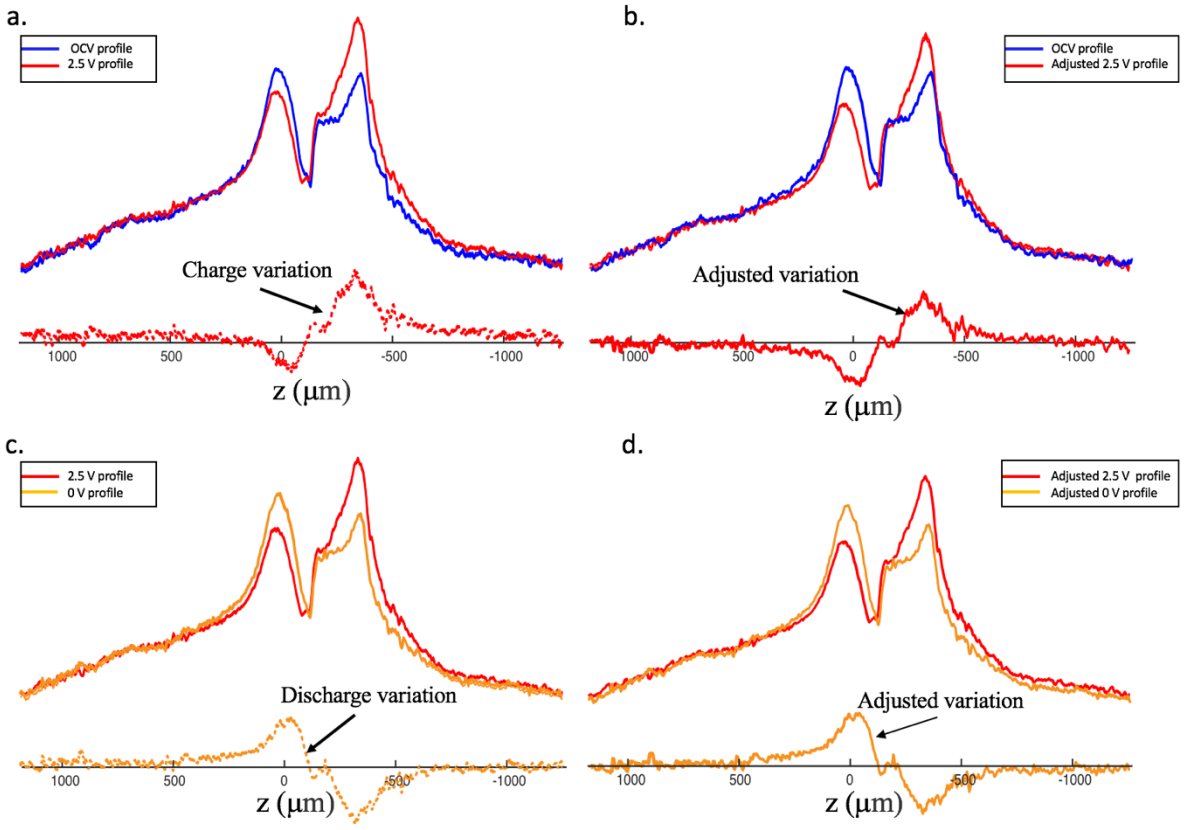

Figure S6. ^{1}H concentration profiles of a supercapacitor under open circuit (blue), at 2.5 V (red) and at 0 V (yellow) after discharge. Concentration variation profiles for charge (a. and b.) and discharge (c. and d.), with no scaling (left) and scaling (right).

Changes in concentration profiles for carbon A and carbon CDC upon charge and discharge

The concentration profile unit is arbitrary. We assumed that the ions do not disappear from the detection zone and we calibrated the total area of all the concentration profiles to be identical for a given cell, as explained above.

The areas of the signals differed between the four cells (slight variations in the amount of electrolyte present in the detection zone, slight variations in the conductivity of the cell). In order to compare the profiles of CC and CDC carbons in Figures 2 and S7 the set of ^{1}H concentration profiles (OCV, 2.5 V, 0 V) for the CC carbons were calibrated to obtain the same area as the ^{1}H concentration profiles for the CDC carbon. A single scaling factor is needed as the 3 profiles (after the processing explained above). The profiles of relative concentration variations are displayed using the same scale as the concentration profiles so that their intensity can be compared. The relative concentration variations are therefore only due to changes in the position (and potentially shift) of the ions.

There is no physical reason for the ^{19}F area to be identical to the ^{1}H area, notably because the ^{19}F NMR detection coil does not have the same sensitivity as the ^{1}H NMR detection coil. Here, the ^{19}F concentration profiles for CC and CDC were calibrated to the same area as the ^{1}H concentration profiles to get comparable relative scales for the differences.

Table S2: Relative scaling factors for the profiles in figure 2 and figure S7

Experiment	CC carbon – ^{1}H (set of 3 profiles)	CDC carbon – ^{1}H (set of 3 profiles)	CC carbon – ^{19}F (set of 3 profiles)	CDC carbon – ^{19}F (set of 3 profiles)
Scaling factor	0.68	1	0.49	0.55

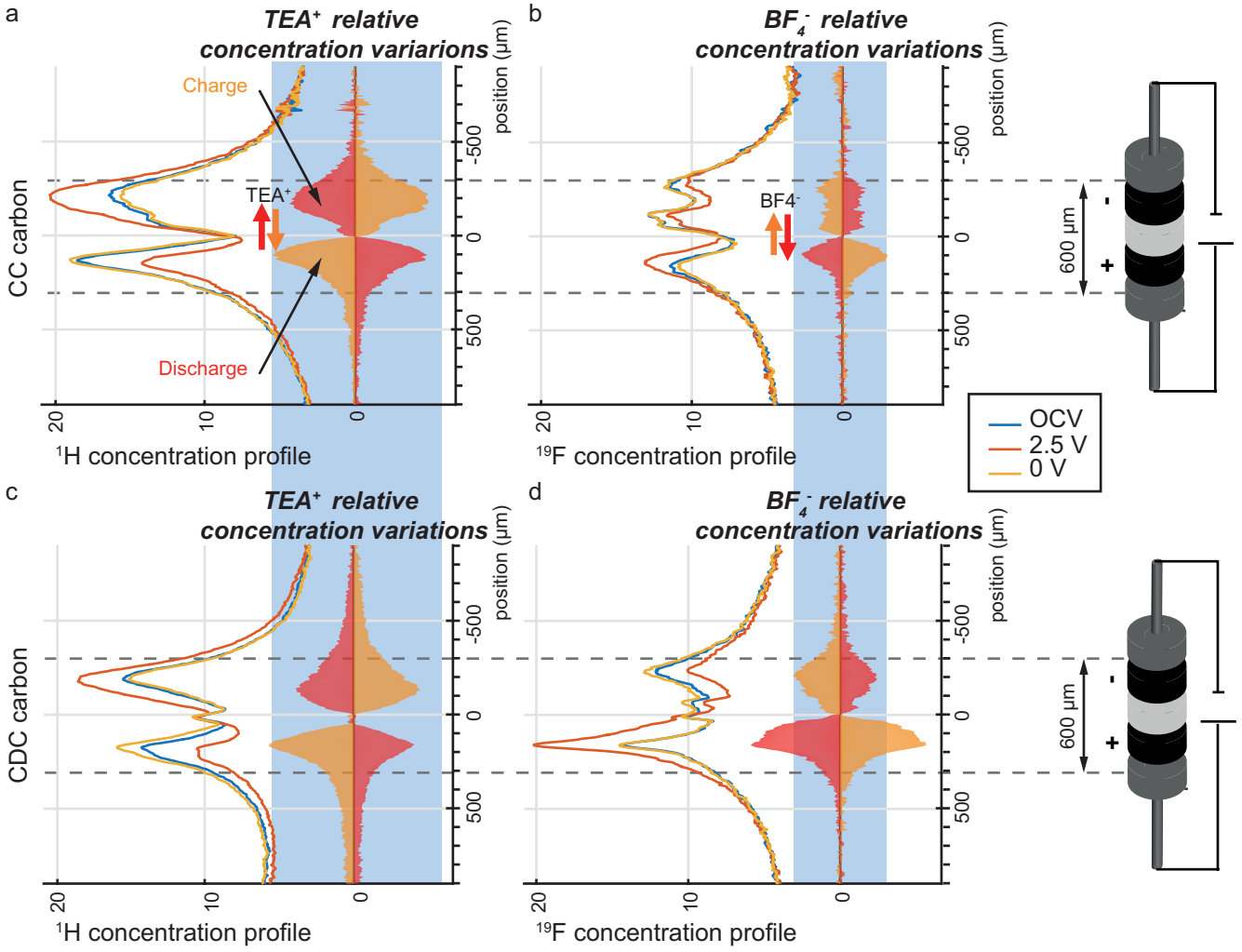

Figure S7. ^{1}H (a,c) and ^{19}F (b,d) 1D concentration profiles of a supercapacitor made of CC (a,b) and CDC (c,d) carbons, during OCV before charging (blue), at 2.5 V (red) and 0 V(yellow). The concentration variations on charge (between 2.5 V and OCV) are displayed on the right of the profiles as filled red curves, and the concentration changes on discharge (between 2.5 V and 0 V) are displayed as filled orange curves.

REFERENCES

(1) Deschamps, M.; Gilbert, E.; Azais, P.; Raymundo-Piñero, E.; Ammar, M. R.; Simon, P.; Massiot, D.; Béguin, F. Exploring Electrolyte Organization in Supercapacitor Electrodes with Solid-State NMR. *Nat. Mater.* **2013**, *12*, 351–358.

(2) Forse, A. C.; Griffin, J. M.; Presser, V.; Gogotsi, Y.; Grey, C. P. Ring Current Effects: Factors Affecting the NMR Chemical Shift of Molecules Adsorbed on Porous Carbons. *J. Phys. Chem. C* **2014**, *118*, 7508–7514.

(3) Wang, H.; Forse, A. C.; Griffin, J. M.; Trease, N. M.; Trognko, L.; Taberna, P.-L.; Simon, P.; Grey, C. P. *In Situ* NMR Spectroscopy of Supercapacitors: Insight into the Charge Storage Mechanism. *J. Am. Chem. Soc.* **2013**, *135*, 18968–18980.

(4) Chmiola, J.; Yushin, G.; Gogotsi, Y.; Portet, C.; Simon, P.; Taberna, P. L. Anomalous Increase in Carbon Capacitance at Pore Sizes Less Than 1 Nanometer. *Science* **2006**, *313*, 1760–1763.

(5) Jagiello, J.; Olivier, J.P. 2D-NLDFT Adsorption Models for Carbon Slit-Shaped Pores with Surface Energetical Heterogeneity and Geometrical Corrugation. *Carbon* **2013**, *55*, 70-80